



## Yrast and non-yrast $2^+$ states of $^{134}\text{Ce}$ and $^{136}\text{Nd}$ populated in relativistic Coulomb excitation

T.R. Saito<sup>a,\*</sup>, N. Saito<sup>a</sup>, K. Starosta<sup>b</sup>, J. Beller<sup>c</sup>, N. Pietralla<sup>c,d,e</sup>, H.J. Wollersheim<sup>a</sup>, D.L. Balabanski<sup>f,h,g</sup>, A. Banu<sup>a,1</sup>, R.A. Bark<sup>i</sup>, T. Beck<sup>a</sup>, F. Becker<sup>a</sup>, P. Bednarczyk<sup>a</sup>, K.-H. Behr<sup>a</sup>, G. Benzoni<sup>j</sup>, P.G. Bizzeti<sup>k</sup>, C. Boiano<sup>j</sup>, A. Bracco<sup>j</sup>, S. Brambilla<sup>j</sup>, A. Brünle<sup>a</sup>, A. Bürger<sup>l</sup>, L. Caceres<sup>a,m</sup>, F. Camera<sup>j</sup>, F.C.L. Crespi<sup>j</sup>, P. Doornenbal<sup>a</sup>, A.B. Garnsworthy<sup>n</sup>, H. Geissel<sup>a</sup>, J. Gerl<sup>a</sup>, M. Górska<sup>a</sup>, J. Grebosz<sup>a,o</sup>, G. Hagemann<sup>p</sup>, J. Jolie<sup>d</sup>, M. Kavatsyuk<sup>a,q</sup>, O. Kavatsyuk<sup>a,q</sup>, T. Koike<sup>r</sup>, I. Kojouharov<sup>a</sup>, N. Kurz<sup>a</sup>, J. Leske<sup>c</sup>, G. Lo Bianco<sup>h</sup>, A. Maj<sup>o</sup>, S. Mallion<sup>s</sup>, S. Mandal<sup>t</sup>, M. Maliage<sup>i</sup>, T. Otsuka<sup>u,v</sup>, C.M. Petrache<sup>h</sup>, Zs. Podolyak<sup>n</sup>, W. Prokopowicz<sup>a</sup>, G. Rainovski<sup>f,e</sup>, P. Reiter<sup>d</sup>, A. Richard<sup>d</sup>, H. Schaffner<sup>a</sup>, S. Schielke<sup>l</sup>, G. Sletten<sup>p</sup>, N.J. Thompson<sup>n</sup>, D. Tonev<sup>w,g</sup>, J. Walker<sup>a,n</sup>, N. Warr<sup>d</sup>, O. Wieland<sup>j</sup>, Q. Zhong<sup>w</sup>

<sup>a</sup> Gesellschaft für Schwerionenforschung (GSI), Darmstadt 64291, Germany

<sup>b</sup> Department of Physics and Astronomy and National Superconducting Cyclotron Laboratory, MSU, East Lansing, MI 48824, USA

<sup>c</sup> Institut für Kernphysik, Technische Universität Darmstadt, Schlossgartenstrasse 9, D-64289 Darmstadt, Germany

<sup>d</sup> Institut für Kernphysik, Universität zu Köln, Zùlpicherstrasse 77, D-50937 Köln, Germany

<sup>e</sup> Department of Physics and Astronomy, SUNY at Stony Brook, NY 11794, USA

<sup>f</sup> Faculty of Physics, St. Kliment Ohridski University of Sofia, 1164 Sofia, Bulgaria

<sup>g</sup> The Institute for Nuclear Research and Nuclear Energy, BAS, 1784 Sofia, Bulgaria

<sup>h</sup> Dipartimento di Fisica dell'Università di Camerino, and INFN Sezione di Perugia, Italy

<sup>i</sup> iThemba LABS, Somerset West 7129, South Africa

<sup>j</sup> Dipartimento di Fisica, Università di Milano and INFN Sezione di Milano, Via Celoria 16, 20133 Milano, Italy

<sup>k</sup> Dipartimento di Fisica dell'Università di Firenze and INFN, Sezione di Firenze, Firenze, Italy

<sup>l</sup> Helmholtz-Institut für Strahlen- und Kernphysik, Universität Bonn, Nussallee 14-16, D-53115, Germany

<sup>m</sup> Departamento de Física Teórica, Universidad Autónoma de Madrid, E-28049 Madrid, Spain

<sup>n</sup> Department of Physics, University of Surrey, Guildford GU2 7XH, United Kingdom

<sup>o</sup> The Niewodniczanski Institute of Nuclear Physics, Polish Academy of Sciences, ul. Radzikowskiego 152, 31-342 Kraków, Poland

<sup>p</sup> The Niels Bohr Institute, Blegdamsvej 17, 2100 Copenhagen, Denmark

<sup>q</sup> National Taras Shevchenko University of Kyiv, 01033 Kyiv, Ukraine

<sup>r</sup> Department of Physics, Tohoku University, 980-8578 Sendai, Japan

<sup>s</sup> University of Leuven, IKS, Celestijnenlaan 200 D, 3001 Leuven, Belgium

<sup>t</sup> Department of Physics and Astrophysics, University of Delhi, New Delhi, India

<sup>u</sup> Department of Physics and Center for Nuclear Study, University of Tokyo, Hongo, Tokyo 113-0033, Japan

<sup>v</sup> RIKEN, Hirosawa, Wako-shi, Saitama 351-0198, Japan

<sup>w</sup> Laboratori Nazionali di Legnaro, Viale dell'Università 2, 35020 Legnaro (PD), Italy

### ARTICLE INFO

#### Article history:

Received 26 October 2007

Received in revised form 16 September 2008

Accepted 16 September 2008

Available online 20 September 2008

Editor: V. Metag

#### PACS:

23.20.En

23.20.Js

25.70.De

27.60.+j

### ABSTRACT

The first  $2^+$  states in  $^{134}\text{Ce}$  and  $^{136}\text{Nd}$  and the second  $2^+$  state in  $^{136}\text{Nd}$  were populated by Coulomb excitation at relativistic energies, and  $\gamma$ -rays were measured using the RISING setup at GSI. For  $^{134}\text{Ce}$  an indication of the excitation to the second  $2^+$  state was observed. This experiment performed for the first time Coulomb excitation to second  $2^+$  states with rare isotope beams at relativistic energies. For  $^{136}\text{Nd}$  the  $B(E2; 2_1^+ \rightarrow 0^+)$ ,  $B(E2; 2_2^+ \rightarrow 0^+)$ , and  $B(E2; 2_2^+ \rightarrow 2_1^+)$  values relative to the previously known  $B(E2; 2_1^+ \rightarrow 0^+)$  value for  $^{134}\text{Ce}$  are determined as 81(10), 11(3) and 180(92) W.u., respectively. The results are discussed in the framework of geometrical models that indicate pronounced  $\gamma$ -softness in these nuclei.

© 2008 Elsevier B.V. All rights reserved.

\* Corresponding author at: GSI, Planckstrasse 1, D-64291 Darmstadt, Germany.  
Tel.: +49 6159 71 2032; fax: +49 6159 71 2809.

E-mail address: t.saito@gsi.de (T.R. Saito).

<sup>1</sup> Present address: Cyclotron Laboratory, Texas A&M University, Texas, USA.

Despite the rotational invariance of the nuclear many body system, triaxial shapes originate from specific long-range correlations. They have represented an intriguing phenomenon in nuclear structure physics for five decades. Quadrupole-deformed nuclear shapes with soft-triaxiality [1,2] and with rigid triaxiality [3] have already been proposed in the 1950's. In the nuclear mass region  $A \sim 130$ , observed low-spin structures have been interpreted in terms of the occurrence of triaxial deformation, predominantly with a high degree of  $\gamma$ -softness. Corresponding nuclear spectra can be satisfactorily described [4] in terms of the corresponding  $O(6)$  dynamical symmetry [5] of the interacting boson model. The properties of the two lowest  $2^+$  states of even-even nuclei are particularly sensitive to a triaxial shape of the nuclear ground state and to the softness of its triaxiality. From theoretical and systematic studies [6,7], it has been suggested that the  $N = 76$  nuclei are more  $\gamma$ -rigid than their neighbors with higher neutron number. At moderate spins, the rotation of a triaxial nucleus may give rise to pairs of identical  $\Delta I = 1$  bands with the same parity—chiral twin bands [8]. In doubly-odd nuclei these structures can arise from the perpendicular coupling of the angular momenta of the valence particles and a triaxial core. The existence of self-consistent rotating mean-field solutions of chiral character has been predicted for the  $N = 75$  nucleus  $^{134}\text{Pr}$  [9], where a pair of bands with the same parity and spin close in excitation energy has already been observed [10]. In a number of nuclei in this region such bands have been observed and interpreted as chiral doublets [11–13].

The measured lifetime [14] and the analysis [15] of the band crossing of the two doublet bands in  $^{134}\text{Pr}$  have put the chiral interpretation for this nucleus to discussion. A recent paper [16] suggests an interpretation of lifetimes and  $\gamma$ -ray branching ratios with theoretical calculations of the two-quasiparticle triaxial rotor and interacting boson–fermion–fermion models in terms of weak chirality dominated by shape fluctuations. In other nuclei, lifetime measurements have corroborated the chiral picture. In the odd-mass nucleus  $^{135}\text{Nd}$  the transition probabilities for intra- and inter-band transitions confirm the chiral character and suggest that the observed behavior is associated with a transition from a chiral vibration to a chiral rotation [17]. It is interesting to study the triaxiality of the even–even nuclei,  $^{134}\text{Ce}$  and  $^{136}\text{Nd}$ , which are the corresponding even–even core of  $^{134}\text{Pr}$  and the direct neighbor of  $^{135}\text{Nd}$ , respectively, by measuring observables that are sensitive to the amount and rigidity of triaxial deformation. Therefore, relativistic Coulomb excitation experiments were performed to populate  $2^+$  states in  $^{134}\text{Ce}$  and  $^{136}\text{Nd}$ . From the decay of the first  $2_1^+$  and second  $2_2^+$  states the  $B(E2)$  values were deduced which yield information on the triaxiality parameter  $\gamma$  within geometrical models such as the Asymmetric Rotor Model (ARM) [2,3] or the Geometric Collective Model (GCM) by Gneuss and Greiner [18] that we will employ below.

Two consecutive experiments were performed to measure Coulomb excitation of high-energy  $^{134}\text{Ce}$  and  $^{136}\text{Nd}$  beams using the FRS-RISING setup at GSI [19]. A primary beam of  $^{152}\text{Sm}$  at 750 A MeV impinged on a 4 g/cm<sup>2</sup>  $^9\text{Be}$  production target at the entrance of the fragment separator (FRS) [20]. Fully stripped secondary beams of  $^{134}\text{Ce}$  and  $^{136}\text{Nd}$  were separated in the FRS by their magnetic rigidity and their specific energy loss in the degraders. The nuclei of interest were identified event-by-event by employing scintillator detectors, a multiple sampling ionization chamber (MUSIC) [21], and multi-wire proportional chambers (MWPC). Two plastic scintillators with a thickness of 3 and 0.5 mm each were mounted at the intermediate and final focal plane and served for the time of flight (TOF) measurement. From the TOF and the flight path length, the velocity of the ions was determined. The energy loss ( $\Delta E$ ) of each ion was provided by the MUSIC chamber and yielded the element number  $Z$ . By combining these measurements, the full in-flight identification of ions in

$Z$  and  $A/Q$  arriving at the final reaction target was achieved. The purity of the secondary  $^{134}\text{Ce}$  and  $^{136}\text{Nd}$  beams is almost 100% with this identification. In addition the incoming trajectories of the ions were measured by two MWPCs. The energies of  $^{134}\text{Ce}$  and  $^{136}\text{Nd}$  beams were around 126 A MeV before impinging on a secondary 386 mg/cm<sup>2</sup> gold target at the final focal plane. Projectiles and target nuclei were mainly excited by the electromagnetic interaction. The de-excitation  $\gamma$ -rays in coincidence with projectile residues were detected by 15 EUROBALL cluster Ge detectors [22]. The cluster Ge detectors were placed at forward angles in order to maximize the effective solid angle by the Lorentz boost and to minimize the Doppler broadening effect. They were arranged in three rings around the beam pipe, with the axis of the central detectors in each ring positioned at 16°, 33°, and 36°. A distance of 700 mm between the Ge detectors and the Au target was necessary to achieve an energy resolution of  $\sim 3\%$  in FWHM after Doppler correction. The identification of the nuclei behind the reaction target was performed by an array of nine position-sensitive  $\Delta E$ - $E$  calorimeter telescopes (CATE) [19] to ensure the necessary conditions for Coulomb excitations. Energy loss was measured with thin (300  $\mu\text{m}$ ) position-sensitive Si detectors, whereas the residual-energy detectors were made of CsI(Tl) scintillators. The CATE array covered a relevant opening angle of 58 mrad at 1426 mm from the target. For the present projectile–target combinations an angular range of about 36 mrad is important for Coulomb excitation. The position sensitivity and the information on the incoming trajectory allowed for the scattering angle determination.

In the analysis, the scattering angle between an in-coming and an out-going particle and the  $\gamma$ -ray emission angle with respect to the direction of the scattered projectile were calculated event-by-event and used for the Doppler correction. The ion velocity behind the target was deduced for each event from TOF taking the energy loss in the Au target into account. The accepted scattering angles in the laboratory frame were limited to the range of 0.8°–1.8° which corresponds to impact parameters in the range of 17–39 fm. At smaller impact parameters nuclear interaction interferes with Coulomb excitation and at larger impact parameters the excitation probability vanishes and the particle– $\gamma$  coincidences are dominated by atomic interactions. For an optimal suppression of atomic background radiation, the analysis required single  $\gamma$ -hit cluster multiplicity for prompt  $\gamma$ -rays at energies in excess of 400 keV in the laboratory frame. Doppler shift corrected  $\gamma$ -ray spectra for  $^{134}\text{Ce}$  and  $^{136}\text{Nd}$  are displayed in Fig. 1. Gamma-rays depopulating the  $2_1^+$  and  $2_2^+$  states are indicated by solid and dashed arrows, respectively. Gamma-rays depopulating the  $2_1^+$  states are observed in both nuclei. The decay of the  $2_2^+$  is also clearly visible in  $^{136}\text{Nd}$ , while only indications are present for the 557 keV and 966 keV transitions in  $^{134}\text{Ce}$ . The excitation energies are already known from former investigations [24]. For the first time, the first and second  $2^+$  states are observed in Coulomb excitation at incident energies larger than 100 A MeV, at least for the case of  $^{136}\text{Nd}$ .

The absolute  $\gamma$ -ray efficiency of the cluster Ge array was determined by a  $\gamma$ - $\gamma$  coincidence measurement between the 1173 keV and 1333 keV transition of a  $^{60}\text{Co}$  source taking into account all combinations of the cluster Ge detectors, combined with the relative efficiency of  $^{152}\text{Eu}$  transitions measured as a function of  $\gamma$ -ray energy, and the efficiency in the rest frame was Lorentz transformed with a velocity parameter of  $v/c = 0.42$  to obtain the absolute efficiency for  $\gamma$ -rays emitted from the moving projectiles. Besides particle– $\gamma$  coincidences, beam particles were also recorded requiring an incoming particle in the last plastic scintillator. From the measured  $\gamma$ -ray intensities the Coulomb excitation cross sections can be determined, that are directly proportional to the reduced transition probabilities. For the analysis and especially for the  $2_2^+ \rightarrow 2_1^+$  transition the  $\gamma$ -ray angular distribution has to be known. Since the intensity of the latter transition was

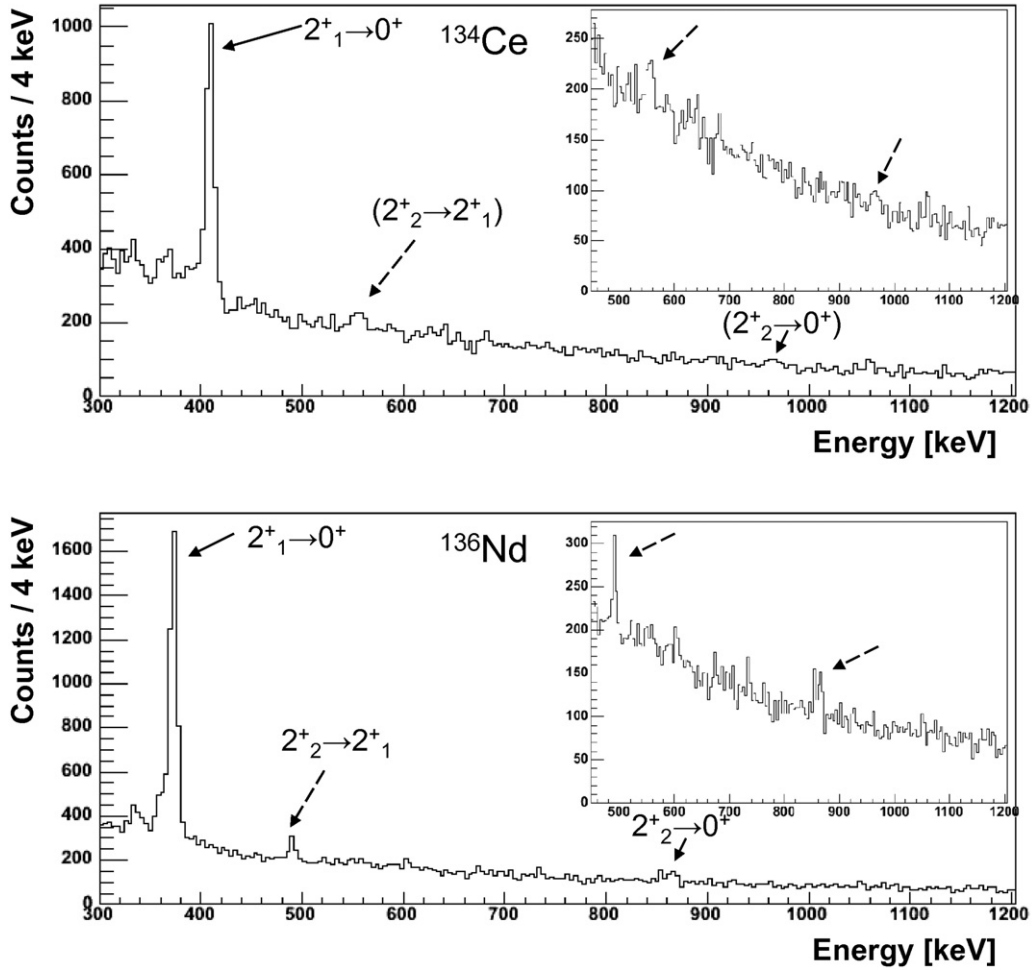


**Fig. 1.** Doppler shift corrected  $\gamma$ -ray spectra for  $^{134}\text{Ce}$  (top panel) and  $^{136}\text{Nd}$  (bottom panel). The insets show the regions with the weak transitions depopulating the second  $2^+$  state. Gamma-rays depopulating the  $2^+_1$  and  $2^+_2$  states are indicated by solid and dashed arrows, respectively.

too weak to be analyzed as a function of the  $\gamma$ -ray emission angle, the  $2^+_1 \rightarrow 0^+$  transition in  $^{134}\text{Ce}$  was used to extract the  $\gamma$ -ray angular distribution and the particle- $\gamma$  angular correlation in order to obtain information on the spin alignment. Our data exhibit a flat angular distribution within statistical fluctuations. One could suppose that such a small alignment could be the result of a substantial feeding from the giant dipole resonance (GDR) states to the  $2^+$  states. However, a typical cross section for GDR states is expected to be on the order of 100 mb and a branching ratio for  $2^+$  feeding with respect to ground state decay is on the order of 1%. Therefore, the distortion of the alignment by the excitation of GDR states should be negligible. From the previous work [25] a clear angular distribution was reported for relativistic Coulomb excitations of  $^{38}\text{S}$  and  $^{40}\text{S}$  with a gold target. The isotropic angular distribution in the current work may be explained as a deorientation of the nuclear spin by hyperfine interactions, due to the longer lifetimes of the  $2^+_1$  states as compared to the sulfur nuclei and due to the presence of one or more bound electrons in the Ce and Nd ions emerging from the gold target. In fact, their velocity  $v \approx 0.42c$  is very close to the classical velocity  $v_0 = (Z/137)c$  of one bound electron in the first Bohr orbit of the ion, while the S ions of Ref. [25] had a velocity much larger than  $v_0$  and were therefore fully stripped. Unfortunately, a quantitative explanation is not available. The data analysis for  $^{136}\text{Nd}$ , hence, assumes a flat angular distribution, according to the experimental observation for  $^{134}\text{Ce}$ .

**Table 1**

$B(E2)$  and  $B(M1)$  values of transitions depopulating the  $2^+_1$  and  $2^+_2$  states in  $^{132}\text{Ba}$ ,  $^{134}\text{Ce}$  and  $^{136}\text{Nd}$ . The values for  $^{134}\text{Ce}$  and  $^{136}\text{Nd}$  are deduced in the present work

Transition	$^{132}\text{Ba}$ $B(E2)$ [W.u.]	$^{134}\text{Ce}$ $B(E2)$ [W.u.]	$^{136}\text{Nd}$ $B(E2)$ [W.u.]
$2^+_1 \rightarrow 0^+$	43(4) <sup>a</sup>	52(5) <sup>a</sup>	80(11)
$2^+_2 \rightarrow 0^+$	3.9(4) <sup>a</sup>	< 11	11(3)
$2^+_2 \rightarrow 2^+_1$	144(14) <sup>a</sup>	< 140	182(93)

<sup>a</sup> From Ref. [24].

In the present work, reduced transition probabilities,  $B(E2)$ , of transitions depopulating the  $2^+_1$  and  $2^+_2$  states of  $^{134}\text{Ce}$  and of  $^{136}\text{Nd}$  were measured relative to the  $B(E2; 2^+_1 \rightarrow 0^+)$  value in  $^{134}\text{Ce}$  which is known to be  $52 \pm 5$  W.u. [23,24]. Following a procedure described in Refs. [26,27], the counts in the  $\gamma$ -ray peaks were normalized to the number of scattered projectiles taking into account the absolute efficiency of the Ge cluster detectors and the deadtime of the data acquisition system (DAQ). From the ratios of these intensities to the  $2^+_1 \rightarrow 0^+$  transition in  $^{134}\text{Ce}$ , the  $B(E2)$  values were determined. Since the relative measurements are free from the major uncertainties of the absolute efficiency calibration for the whole setup [26,27], this method was employed in the present work. The results are listed in Table 1. For the transitions depopulating the  $2^+_2$  state of  $^{134}\text{Ce}$  only an upper limit of the  $B(E2)$  values could be determined. The value takes into account the known  $2^+_2 \rightarrow 2^+_1/0^+$   $\gamma$ -decay branching ratio [24]. The

decay of the  $2_2^+$  state proceeds via a pure E2 transition to the ground state. The  $2_2^+ \rightarrow 2_1^+$  transition in  $^{134}\text{Ce}$  is known to be of E2 character to  $99.1_{-1.3}^{+0.9}\%$  [28]. Therefore, a pure E2 transition was assumed for the transition depopulating the  $2_2^+$  state in  $^{134}\text{Ce}$  as well as in  $^{136}\text{Nd}$ . Since Coulomb excitation of the  $^{197}\text{Au}$  target was also observed,  $B(E2)$  values of the observed transitions in  $^{134}\text{Ce}$  and  $^{136}\text{Nd}$  could be deduced by normalizing to the one of the  $7/2^+ \rightarrow 3/2^+$  transition of  $^{197}\text{Au}$  by taking into account the absolute efficiency of EUROBALL cluster Ge detectors for  $\gamma$ -rays emitted at rest in the laboratory frame and the Coulomb excitation cross section for  $^{197}\text{Au}$ . Deduced  $B(E2)$  values are 77(26), 97(27), 13(5) and 219(124) W.u. for transitions of  $2_1^+ \rightarrow 0^+$  in  $^{134}\text{Ce}$ ,  $2_1^+ \rightarrow 0^+$ ,  $2_2^+ \rightarrow 0^+$  and  $2_2^+ \rightarrow 2_1^+$  in  $^{136}\text{Nd}$ , respectively, which are consistent within errors with the values shown in Table 1 and validate our data analysis. The E2 transition strengths of 43–80 W.u. for the  $2_1^+ \rightarrow 0^+$  yrast transitions in the  $N = 76$  isotones  $^{132}\text{Ba}$ ,  $^{134}\text{Ce}$ , and  $^{136}\text{Nd}$  suggest a comparison with a collective nuclear model. From the  $B(E2; 2_1^+ \rightarrow 0_1^+)$  values, the intrinsic quadrupole moments  $Q_0$  and the axial  $\beta$  deformation could be estimated if one assumed applicability of the axially-symmetric rigid-rotor relations. The corresponding values would be  $Q_0 = 3.0, 3.3, 4.2$  [eb] and the deformation parameters  $\beta = 0.19, 0.20, 0.24$  for  $^{132}\text{Ba}$ ,  $^{134}\text{Ce}$ , and  $^{136}\text{Nd}$ , respectively. Deviations of the nuclear shape from axial symmetry are observed from the excitation energy ratio of the second  $2_2^+$  to the first excited  $2_2^+$  state. In the rigid asymmetric rotor model (ARM) [3] the excitation energy ratio  $E(2_2^+)/E(2_1^+)$  is given by

$$\frac{E(2_2^+)}{E(2_1^+)} = \frac{3 + \sqrt{9 - 8 \cdot \sin^2(3\gamma)}}{3 - \sqrt{9 - 8 \cdot \sin^2(3\gamma)}}.$$

The  $\gamma$  deformation parameters for  $^{132}\text{Ba}$ ,  $^{134}\text{Ce}$ , and  $^{136}\text{Nd}$  derived from this relation would result in  $\gamma = 26.3^\circ, 25.3^\circ$ , and  $25.7^\circ$ , respectively. For these calculations, the  $B(E2)$  ratios were calculated from the intensity ratio of the two transitions depopulating the  $2_2^+$  state, which is given in Ref. [24]. These  $\gamma$  deformation parameters can be compared with the ratio of  $B(E2)$  values through the following equation

$$\frac{B(E2; 2_2^+ \rightarrow 2_1^+)}{B(E2; 2_2^+ \rightarrow 0^+)} = \frac{20}{7} \frac{\frac{\sin^2(3\gamma)}{9 - 8 \cdot \sin^2(3\gamma)}}{1 - \frac{3 - 2 \cdot \sin^2(3\gamma)}{\sqrt{9 - 8 \cdot \sin^2(3\gamma)}}}$$

within the ARM framework. In Fig. 2 the ratio of  $B(E2)$  values connecting the  $2_2^+$  decay transitions are plotted versus the energy ratio  $E(2_2^+)/E(2_1^+)$  for  $^{134}\text{Ce}$  and  $^{136}\text{Nd}$  together with  $^{132}\text{Ba}$ . The experimental data are compared with predictions of the  $\gamma$ -rigid [3] (dashed line) and  $\gamma$ -soft [2] (solid line) ARM. In a soft nucleus rotational motions are closely connected with intrinsic vibrations of the nuclear surface. Therefore, the nucleus is stretched under rotation, which leads to a change of the  $\beta$  and  $\gamma$  deformation parameters. To account for this effect Davydov developed the soft asymmetric rotor model [2] in which the additional parameter  $\mu$  characterizes the deformability of the surface. For  $\mu = 0$  the nucleus has a perfect rigid shape. It can be seen from Fig. 2 that only the soft ARM ( $\mu \sim 0.5, \gamma \sim 23^\circ$ ) predicts quite satisfactorily the experimental data of  $^{134}\text{Ce}$  and  $^{136}\text{Nd}$ , while  $^{132}\text{Ba}$  seems to be more  $\gamma$  rigid.

However, the energy staggering

$$S(I) = \frac{E(I) - E(I-1)}{E(I+1) - E(I-1)} - \frac{I}{2I+1}$$

of the quasi- $\gamma$  band predicted by the ARM is opposite in phase to those observed for the  $N = 76$  isotones [ $S_{^{134}\text{Ce}}(3_1^+) = +0.187$ ,  $S_{^{134}\text{Ce}}(4_2^+) = -0.054$ ,  $S_{^{136}\text{Nd}}(3_1^+) = +0.113$ ,  $S_{^{136}\text{Nd}}(4_2^+) = -0.063$ ].

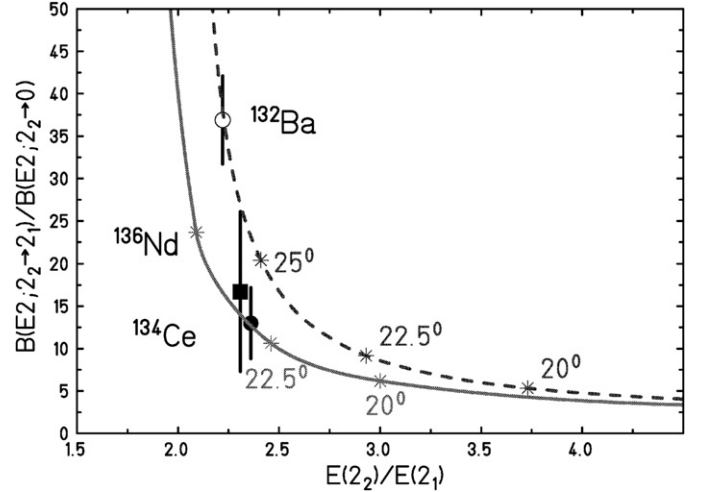


Fig. 2. Ratio of  $B(E2)$  values connecting the  $2_2^+$  decay transitions as a function of the energy ratio  $E(2_2^+)/E(2_1^+)$ . The data of  $^{132}\text{Ba}$  ( $\circ$ ),  $^{134}\text{Ce}$  ( $\bullet$ ) and  $^{136}\text{Nd}$  ( $\blacksquare$ ) are compared with predictions of the  $\gamma$ -rigid (dashed line) and  $\gamma$ -soft ( $\mu = 0.5$ ) asymmetric rotor model [2,3]. The asterisk denote the theoretical results which are calculated in steps of  $2.5^\circ$  in  $\gamma$ .

The experimental staggering hints at a considerable degree of  $\gamma$ -softness. Complete  $\gamma$ -independence of the potential would result in  $O(5)$  symmetry [1,5] which yields the maximum energy staggering  $S_{O(5)}(3_1^+) = +0.571$  and  $S_{O(5)}(4_2^+) = -0.444$ . These values have the right phase but are too extreme.

In order to characterize the quadrupole shape of  $^{136}\text{Nd}$  and  $^{134}\text{Ce}$  we have performed GCM calculations with the potential  $V(\beta, \gamma) = V_0[\beta^2 + c_3\beta^3 \cos(3\gamma) + c_4\beta^4 + c_6\beta^6 \cos^2(3\gamma)]$ . The parameters were adjusted for simultaneous description of the ground band energies, the  $E(2_2^+)/E(2_1^+)$  energy ratio, the E2 branching ratio of the  $2_2^+$ , and the energy staggering of the quasi- $\gamma$  band.

Fig. 3 compares the low-energy level scheme of  $^{136}\text{Nd}$  to the GCM results for potential parameters  $V_0 = -2.125$  MeV;  $c_3 = 0.112$ ;  $c_4 = -9.874$  and  $c_6 = -10.345$ . The agreement with the experiment is satisfactory except for the moment of inertia of excited bands, as must be expected for geometrical models without intrinsic degrees of freedom. The calculated staggers,  $S_{\text{GCM}, ^{136}\text{Nd}}(3_1^+) = +0.137$  and  $S_{\text{GCM}, ^{136}\text{Nd}}(4_2^+) = -0.022$  do not depend on a scaling factor for the Moments of Inertia and are close to the experimental values. Panels (c) and (d) show the potential energy as a function of the deformation variables. The potential exhibits a shallow minimum at  $\beta_{\text{min}} = 0.225$ ,  $\gamma_{\text{min}} = 20.6^\circ$  with pronounced  $\gamma$ -softness. Our GCM fits show that a similar description holds for  $^{134}\text{Ce}$ . We conclude that the region of  $\gamma$ -soft nuclei extends from the Xe, Ba-region [4,30,31] well up to  $^{136}\text{Nd}$  at least. The even-even nuclei,  $^{134}\text{Ce}$  and  $^{136}\text{Nd}$ , are not sufficiently  $\gamma$ -rigid to serve as rigid triaxial cores of neighboring odd-odd nuclei in order to sustain chiral geometry without shape-polarizing effects from the unpaired nucleons. In turn, a possible observation of chiral structures in the particle-core coupled neighbors to  $^{134}\text{Ce}$  or  $^{136}\text{Nd}$  must be considered as direct evidence for these shape-polarizing effects.

In summary, the  $B(E2; 2_1^+ \rightarrow 0^+)$  in the  $^{134}\text{Ce}$  and  $^{136}\text{Nd}$  nuclei,  $B(E2; 2_2^+ \rightarrow 0^+)$ , and  $B(E2; 2_2^+ \rightarrow 2_1^+)$  values in the  $^{136}\text{Nd}$  nucleus were measured for the first time by relativistic Coulomb excitation. The comparison with the asymmetric rotor model and the Geometrical Collective Model yields information on the nuclear shape, namely the  $\beta$  and  $\gamma$  quadrupole deformation parameters. It is found that the data hint at a pronounced  $\gamma$ -softness of the  $N = 76$  isotones even up to  $^{136}\text{Nd}$ .



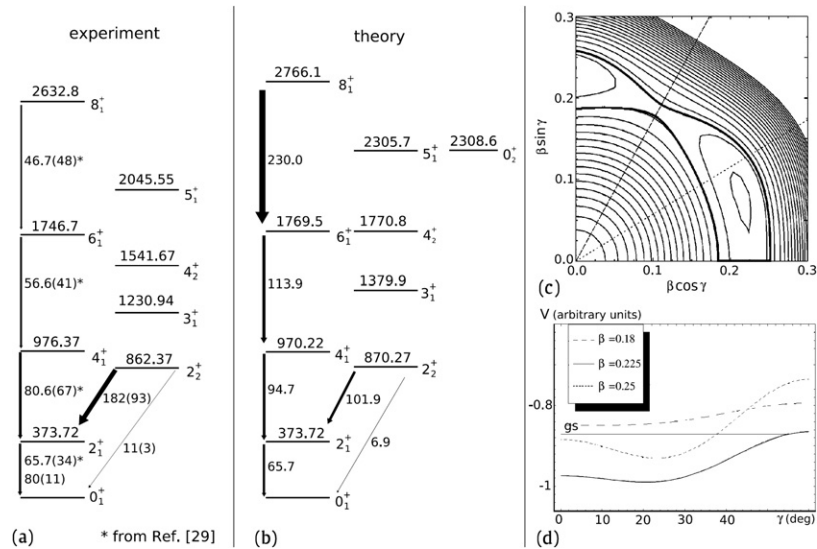


**Fig. 3.** Theoretical description of the low-energy level scheme of  $^{136}\text{Nd}$  (a) with the GCM (b). Excitation energies are given in keV and E2 strengths in W.u. The experimental values indicated with “\*” are taken from Ref. [29]. Panel (c) shows the potential energy surface used for the calculation as a function of the shape variables. The bold line denotes the ground state energy. Cross sections of the potential energy surface for three different values of the deformation parameter  $\beta$  are shown in panel (d) as a function of  $\gamma$ . Substantial  $\gamma$ -softness is obvious.

## Acknowledgements

The authors would like to thank the accelerator department at GSI for their technical support during the experiment. Authors also wish to acknowledge the department of computing and experiment electronics (I.T. and E.E.) for their support on the data acquisition system and the go4 software. D.L. Balabanski was supported in part by the Bulgarian Science Fund, grant VUF05/06. J. Beller and N. Pietralla acknowledge support from the German DFG under Grant SFB 634. A. Bürger acknowledges the support by German BMBF grant No. 06BN-109. A. Maj acknowledges partial financial support by the Polish Ministry of Education and Science, Grant No. 1 P03B030 30. N. Pietralla and G. Rainovski acknowledge support by the USA DOE, Grant No. DE-FG02-04ER41334. P. Reiter was supported by German BMBF grant No. 06K-167.

## References

- [1] L. Wilets, M. Jean, Phys. Rev. 102 (1956) 788.
- [2] A.S. Davydov, A.A. Chaban, Nucl. Phys. 20 (1960) 499.
- [3] A.S. Davydov, G.F. Filippov, Nucl. Phys. 8 (1958) 237.
- [4] R.F. Casten, P. von Brentano, Phys. Lett. B 152 (1985) 22.
- [5] A. Arima, F. Iachello, Phys. Rev. Lett. 40 (1978) 385; A. Arima, F. Iachello, Ann. Phys. (N.Y.) 123 (1979) 468.
- [6] M.O. Kortelahti, et al., Phys. Rev. C 42 (1990) 1267.
- [7] B.D. Kern, et al., Phys. Rev. C 36 (1987) 1514.
- [8] S. Frauendorf, J. Meng, Nucl. Phys. A 617 (1997) 131.
- [9] V.I. Dimitrov, S. Frauendorf, F. Donau, Phys. Rev. Lett. 84 (2000) 5732.
- [10] C.M. Petrache, et al., Nucl. Phys. A 597 (1996) 106.
- [11] K. Starosta, et al., Phys. Rev. Lett. 86 (2001) 971.
- [12] D.J. Hartley, et al., Phys. Rev. C 64 (2001) 031304(R).
- [13] T. Koike, K. Starosta, C.J. Chiara, D.B. Fossan, D.R. LaFosse, Phys. Rev. C 67 (2003) 044319.
- [14] D. Tonev, et al., Phys. Rev. Lett. 96 (2006) 052501.
- [15] C.M. Petrache, G. Hagemann, I. Hamamoto, K. Starosta, Phys. Rev. Lett. 96 (2006) 112502.
- [16] D. Tonev, et al., Phys. Rev. C 76 (2007) 044313.
- [17] S. Mukhopadhyay, et al., Phys. Rev. Lett. 99 (2007) 172501.
- [18] G. Gneuss, W. Greiner, Nucl. Phys. A 171 (1971) 449.
- [19] H.J. Wollersheim, et al., Nucl. Instrum. Methods A 537 (2005) 637.
- [20] H. Geissel, et al., Nucl. Instrum. Methods B 70 (1992) 286.
- [21] R. Schneider, A. Stolz, Technical Manual Ionisation Chamber MUSIC80, 2000.
- [22] J. Eberth, et al., Nucl. Instrum. Methods A 369 (1996) 135.
- [23] D. Husar, et al., Nucl. Phys. A 292 (1977) 267.
- [24] National Nuclear Data Center, <http://www.nndc.bnl.gov>.
- [25] A.D. Davies, et al., Phys. Rev. Lett. 96 (2006) 112503.
- [26] A. Bürger, et al., Phys. Lett. B 622 (2005) 29.
- [27] A. Banu, et al., Phys. Rev. C 72 (2005) 061305(R).
- [28] A. Gade, et al., Nucl. Phys. A 673 (2000) 45.
- [29] G. Kemper, Dissertation, Univ. zu Köln, 2000, <http://kups.uni-koeln.de/volltexte/2003/523/>.
- [30] O. Vogel, et al., Phys. Rev. C 53 (1996) 1660.
- [31] R.A. Meyer, et al., Phys. Rev. C 14 (1976) 2024.